Stellar atmospheres: Application to interferometry

Markus Wittkowski
(ESO)

Outline

- Introduction
- Overview of applications of interferometry
- The limb-darkening effect
  - Basics
  - Example 1 : Comparisons of interferometric data of red giants to PHOENIX model atmospheres to probe the limb-darkening effect
- Extended atmospheres and molecular layers of AGB stars
  - Basics
  - Example 2: Comparisons of data of Mira-variable AGB stars to CODEX model atmospheres

Introduction

From model atmosphere predictions to interferometric observables

- An “atmospheric model” often means the temperature and density stratification of the atmosphere, i.e. the variation of temperature and pressure with height in the atmosphere.
- In addition there may be horizontal temperature and density variations/inhomogeneities (e.g. due to rotation, magnetic fields or convection).
- Together with opacities, stellar model atmospheres predict the spectrum emerging from every point of a stellar disk.
- Most often, model atmospheres are compared to and calibrated by integrated stellar spectra

From model atmosphere predictions to interferometric observables

- Spatially resolved observations can measure the intensity profile across the stellar disk and can go beyond this principal test of model atmospheres.
  - Direct observations of the sun
  - Interferometric observations of stars

The limb-darkened sun with sun spots and Venus. Source: Wikipedia

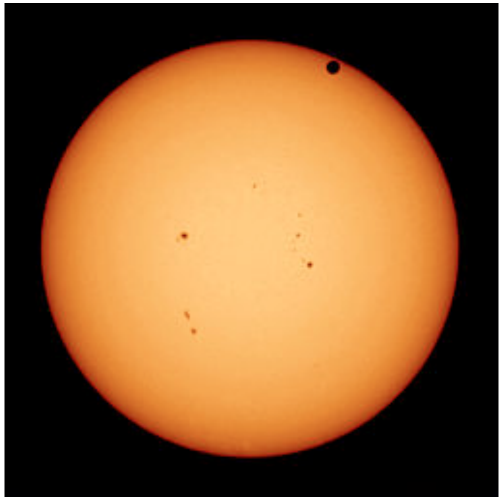

From model atmosphere predictions to interferometric observables

Different ways to compare model atmospheres and observations:

- Based on model-predicted temperature and density stratification:

  Take/reconstruct an image of the star and use opacities to reconstruct the temperature and density stratifications, and compare those to model atmospheres

- Based on model-predicted intensity profiles:

  Take/reconstruct an image of the star and compare it to the intensity profile predicted by the model atmosphere

- Based on model-predicted visibilities:

  Compute synthetic visibility values based on the model atmosphere and compare those to observed visibilities

Images and Visibilities

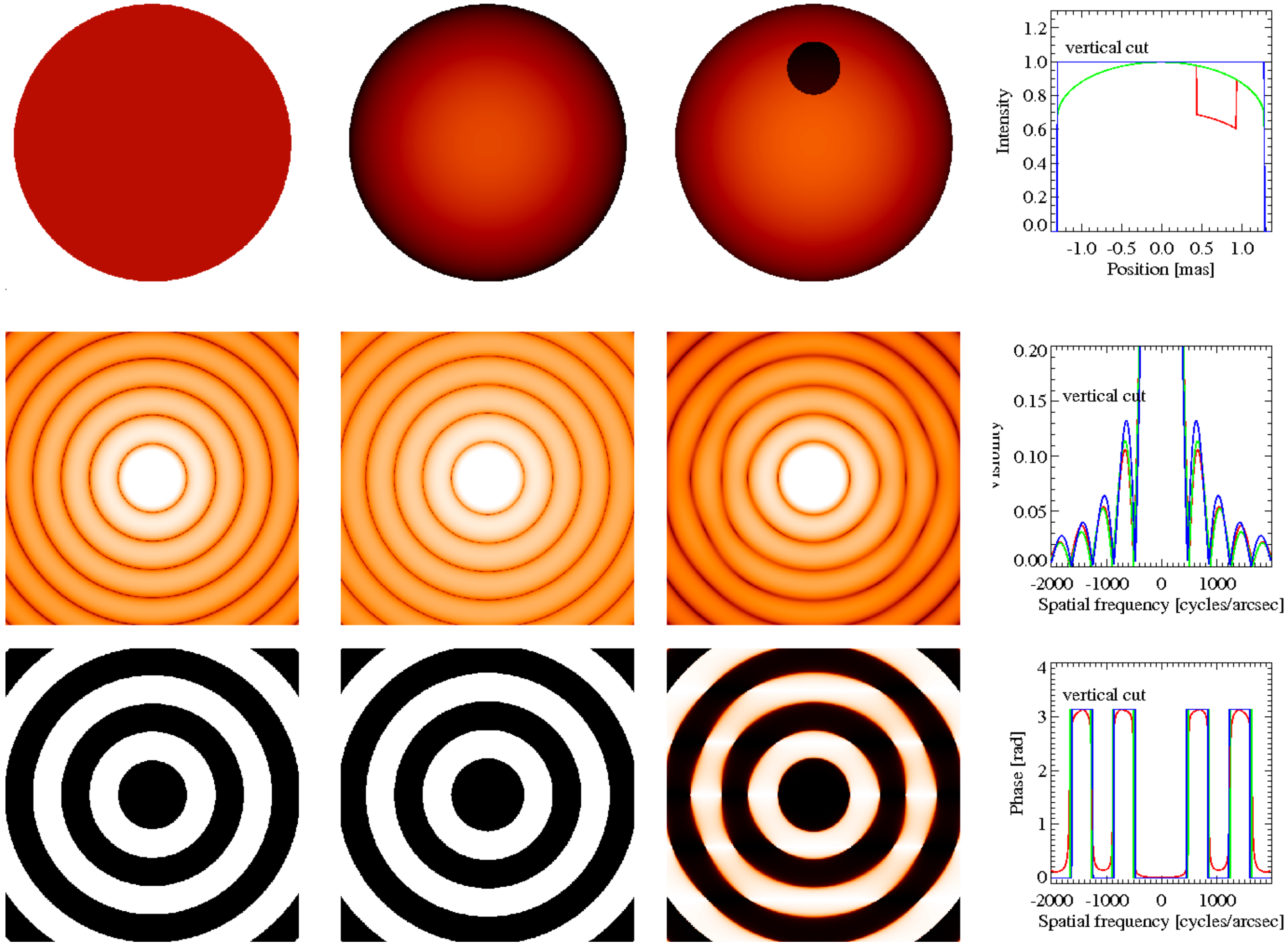

From Wittkowski et al. 2002

Overview of interferometric applications

Optical interferometry and stellar atmospheres

- Limb-darkening effect:
  - Stars appear dimmer near the stellar limb and brighter toward the stellar center.
  - Using interferometry we can resolve the stellar disc and measure the limb-darkening effect, constraining stellar atmosphere models

  → Details later in this presentation

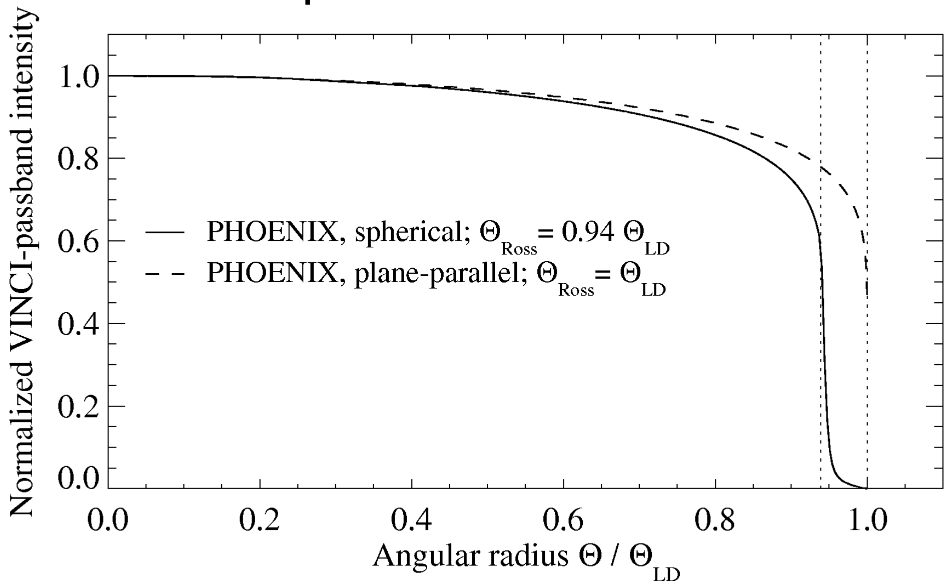

Optical interferometry and stellar atmospheres

- Complex center-to-disc-intensity variations (CLVs) due to pulsations and molecular layers
  - Intensity profiles can be much more complex than a simple limb-darkened disk, due to extended atmospheres including molecular layers (MOLsphere)
  - Difficult definition of the stellar radius

  →Details later in this presentation

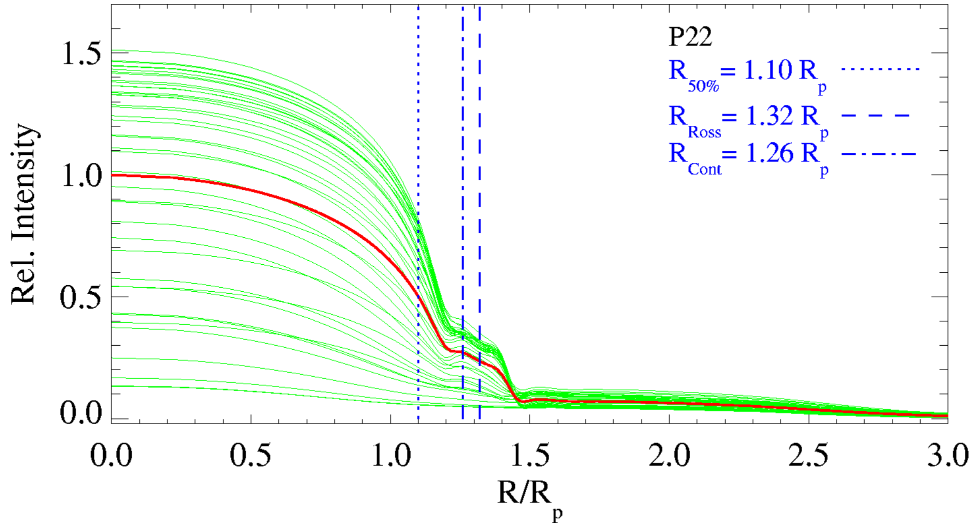

From Fedele et al. 2005

Interferometry and stellar atmospheres

- Photospheric convection and 3D model atmospheres

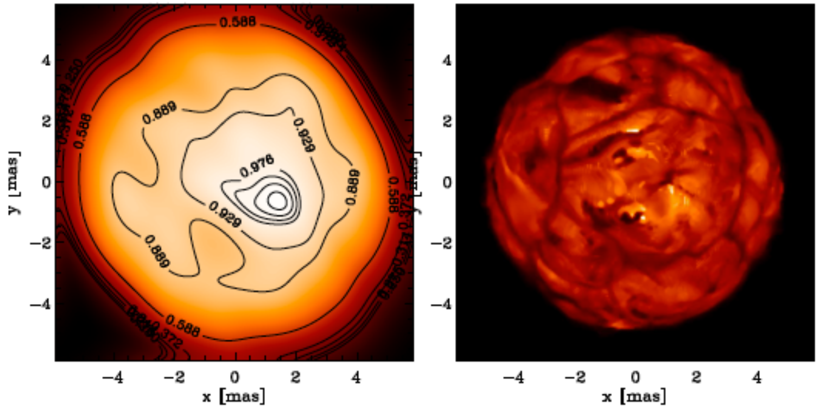

RSG simulation at 1.6 mm (right) and convolution to ~5 mas PSF obtained with the VLTI (left).

Fig. from Chiavassa et al. 2010

Comparison to observations:

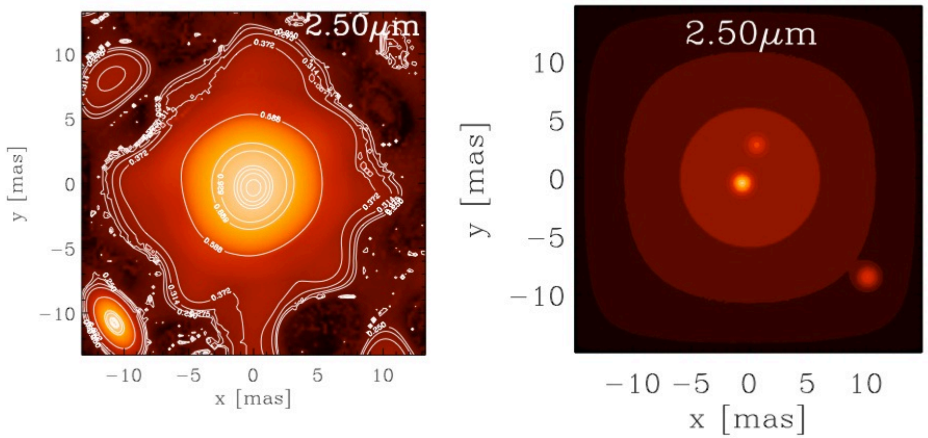

Reconstructed image (left) compared to a geometric model (right).

Fig. from Chiavassa et al. 2010

Interferometry and stellar atmospheres

- Magnetic activity and starspots
  - Surface inhomogeneities caused by magnetic fields

  →Tuesday (D. Shulyak/ A.Domiciano de Souza)

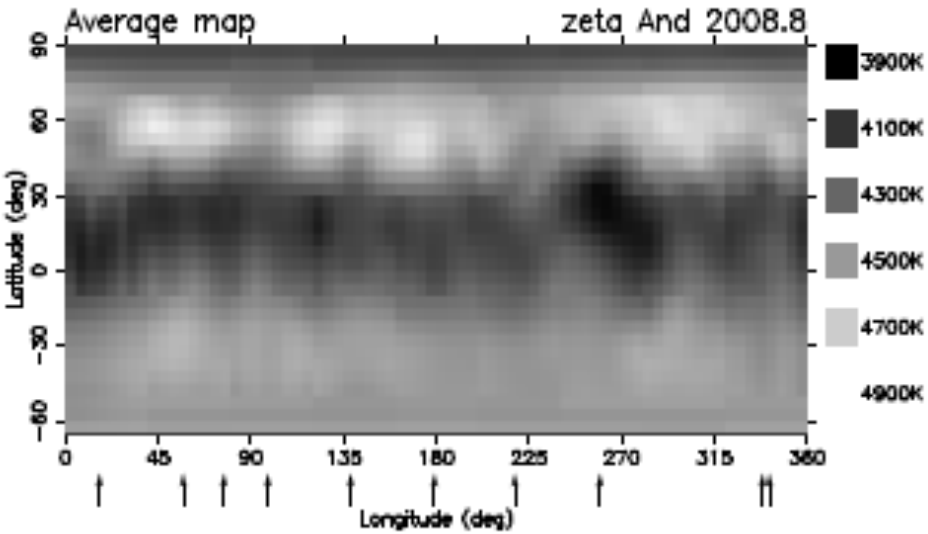

Doppler imaging of the K giant primary of the RSCVn binary ζ And

Fig. from Korhonen et al. 2010

Optical interferometry and stellar atmospheres

- Stellar rotation
  - Oblate stellar shapes
- Gravity darkening: *a pole-to-equator effective temperature gradient resulting from rapid rotation. Local T_{eff} on surface correlates with local gravity (e.g., Teff $\propto g^{1/4}$)*
- → Tuesday (F. Espinosa Lara, A. Domiciano de Souza)

Fig. from Domiciano de Souza et al. 2003

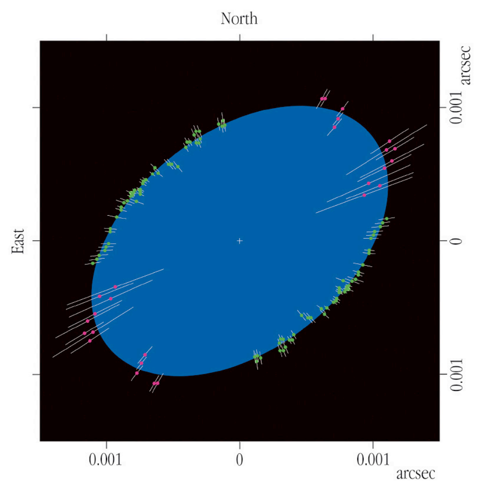

VLTI observation of the fast rotator Achernar

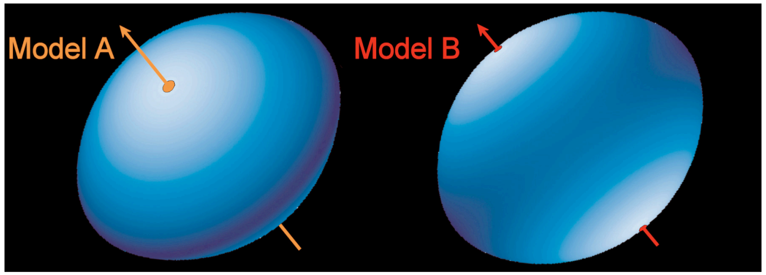

Optical interferometry and stellar atmospheres

- Stellar pulsation
  -> Wednesday/Thursday (O. Creevey)

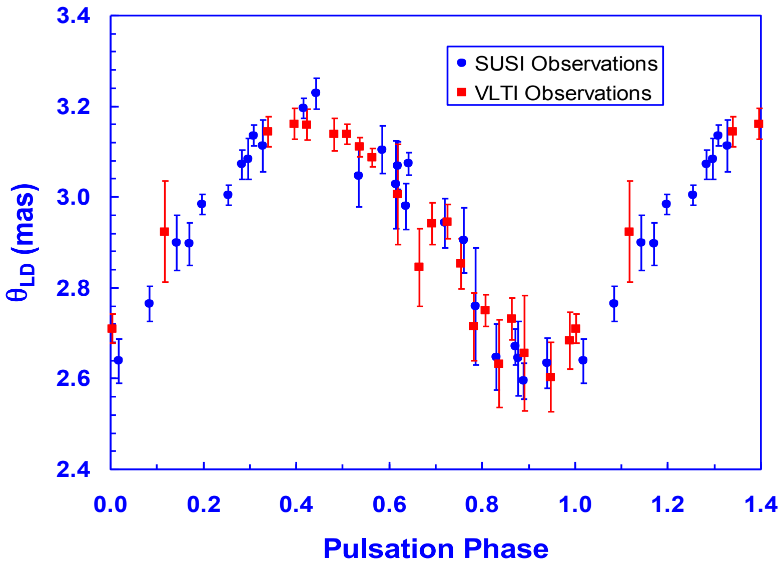

Cepheid
From Kervella et al. (2004)

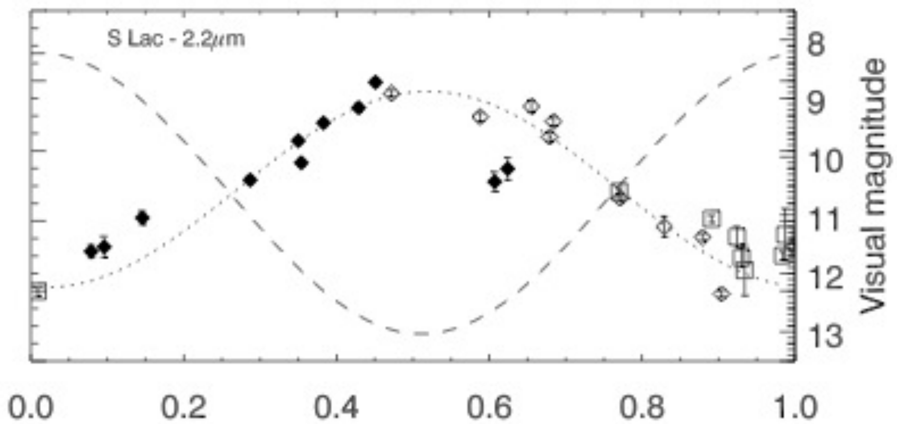

Mira-Variable
From Thompson et al. 2002

Optical interferometry and stellar atmospheres

- Dust formation zones in evolved stars and the circumstellar environment

  Characterization of dust shell parameters such such as inner dust radii, dust chemistry, optical depth.

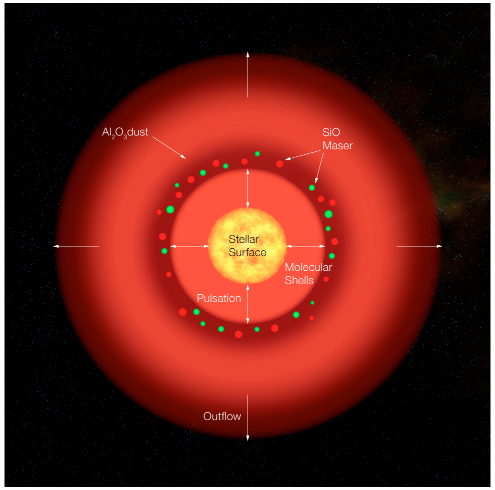

Mira variable.
Based on Wittkowski et al. 2007

Cepheid.
Based on Kervella et al. 2006

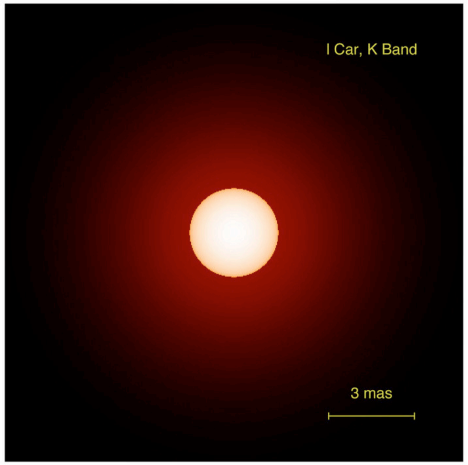

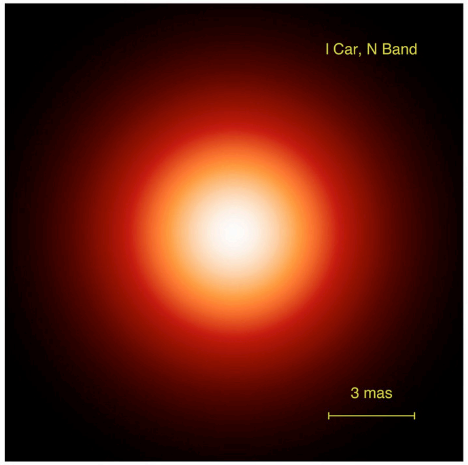

Optical interferometry and stellar atmospheres

- Disks in binary post-AGB stars and shaping mechanisms

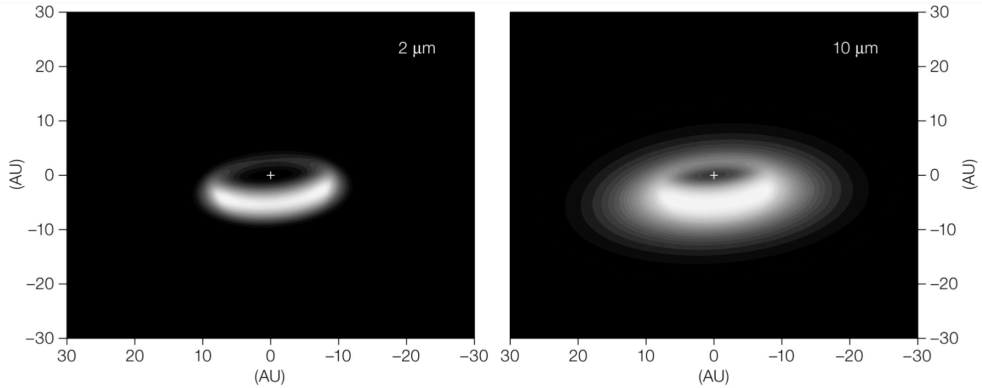

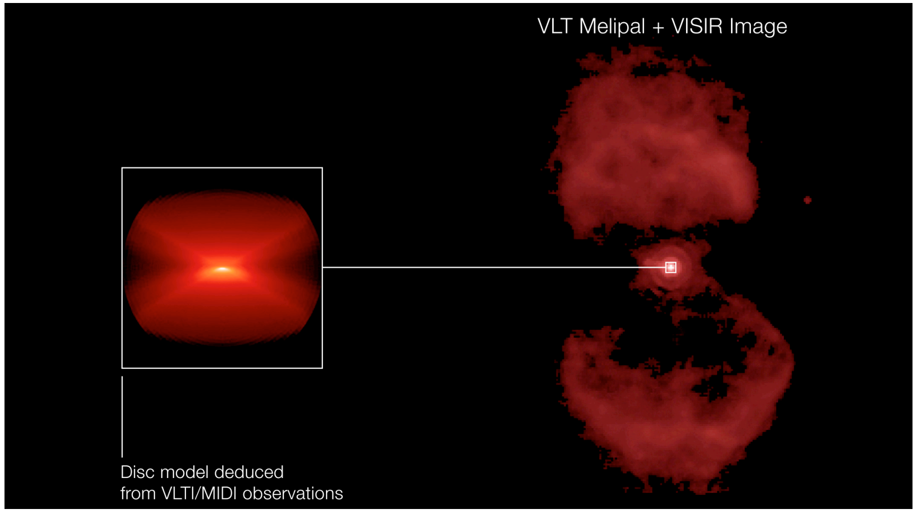

Circumbinary disk around the post-AGB binary IRAS 08544-4431. From Deroo et al. 2007

Ant nebula. From Chesneau et al. 2007

The limb-darkening effect

PHOENIX model atmospheres

Stellar limb darkening

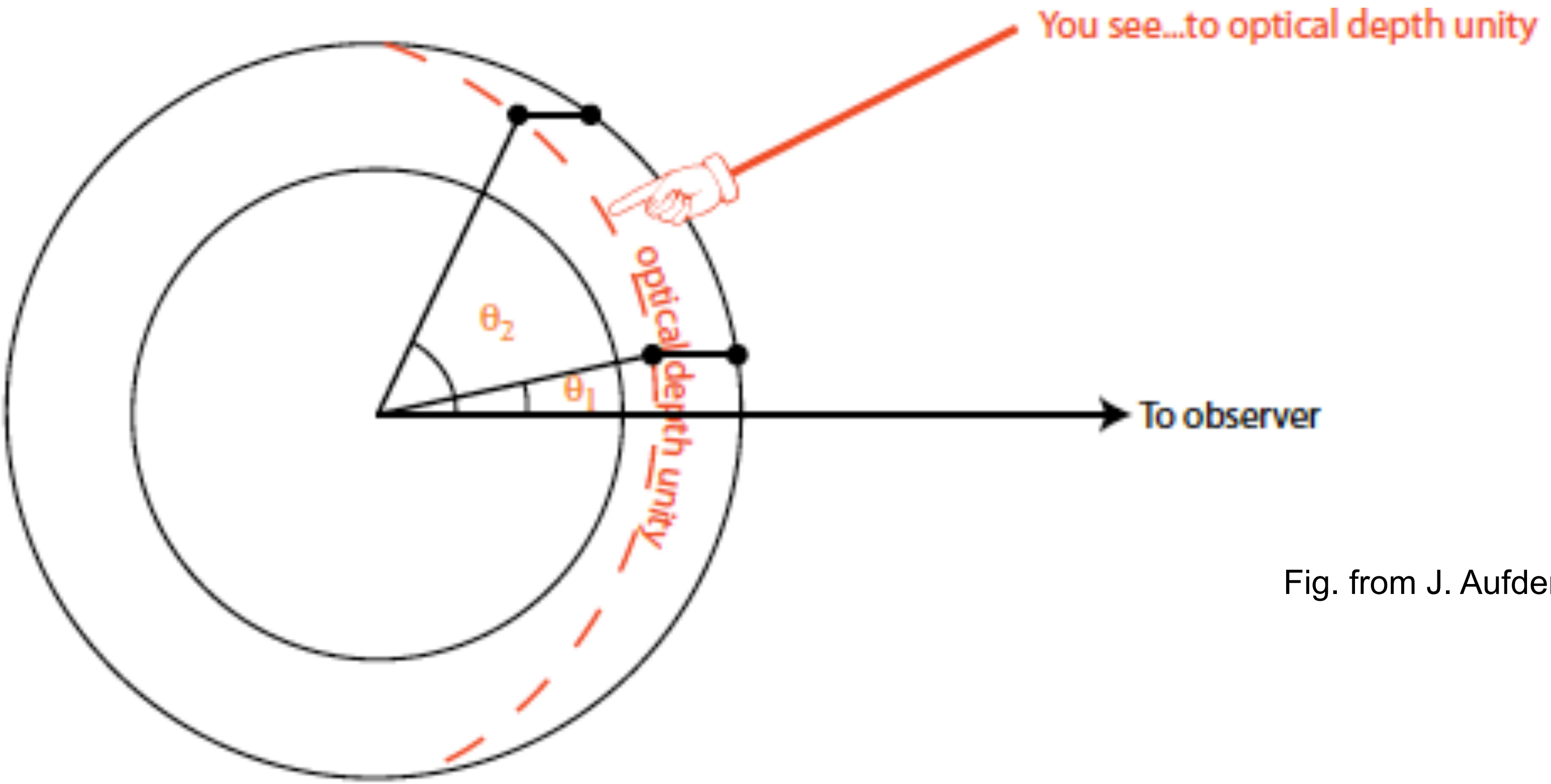

Fig. from J. Aufdenberg

Deeper hotter layers are visible near the disc centre.

Shallower cooler layers are visible near the disc limb.

Geometry of the model atmosphere

- Plane-parallel geometry:

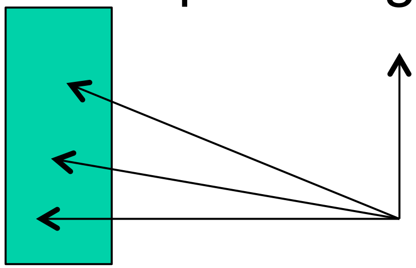

The plane-parallel model is semi-infinite for all viewing angles, i.e. all paths are optically thick.
It has a singularity at a viewing angle of 90 deg, where the intensity profile drops suddenly to 0.

- Spherical geometry:

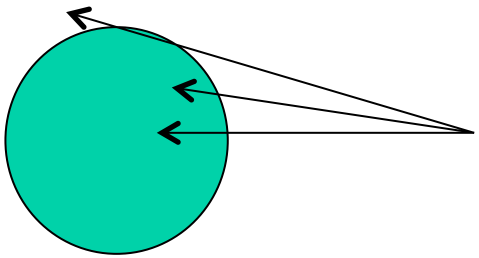

The spherical model has an optically-thin limb.
This causes an inflection point of the intensity profile and a tail-like extension

See Wittkowski et al. (2003, Sect. 3.4)

- Molecular shell scenario

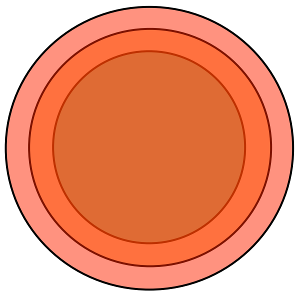

The intensity profile is very complex and wavelength-dependent, with tail-like extensions and multiple components.

Geometry of the model atmosphere

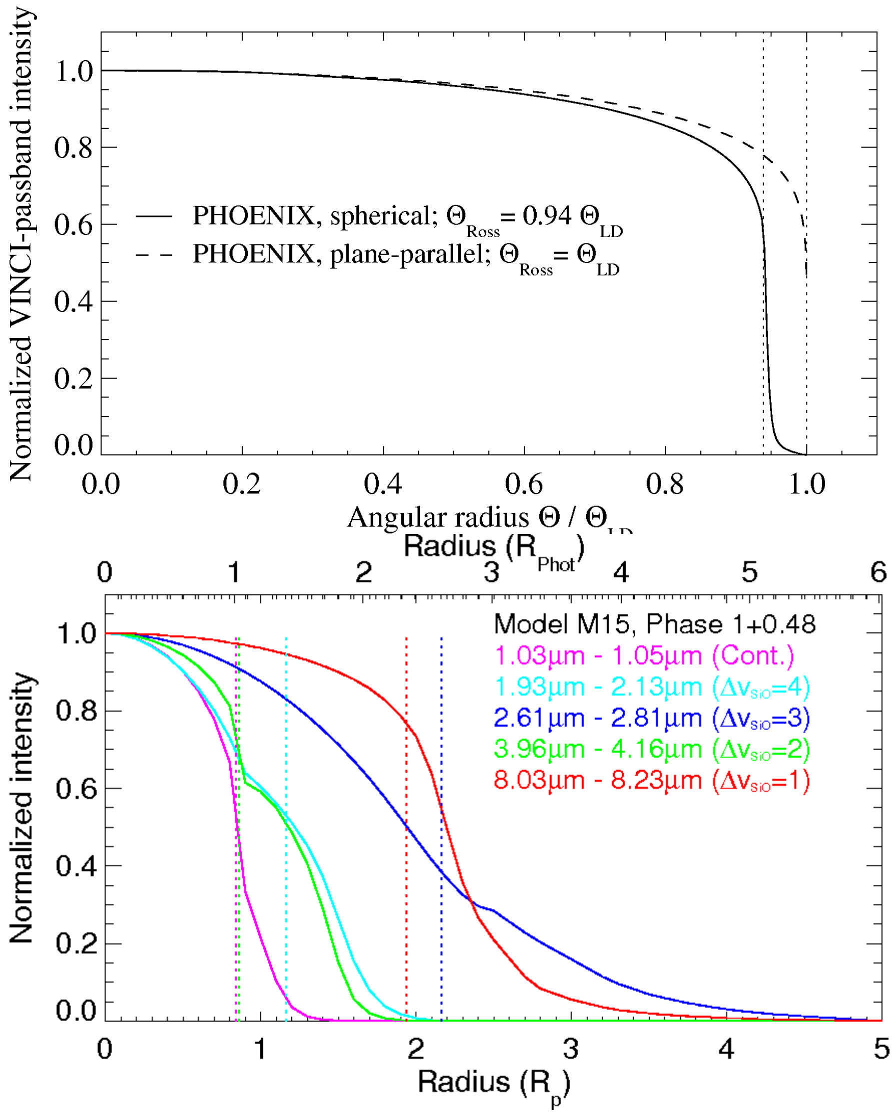

Plane-parallel versus spherical model geometry

More complex intensity profiles with the presence of molecules (water vapour and CO) in extended atmospheric layers/ the *molsphere*

Radius definitions

- 0% intensity radius:
  - Where the intensity profile drops to 0.
  - This is the result of a fit of interferometric data to model atmospheres.
  - Problem: The intensity profile drops to 0 only for a plane-parallel model. For a spherical model, it never drops to 0, and is set to 0 at an arbitrary outer boundary condition.
- 50% intensity radius
  - Where the intensity profile drops to 50% (or any other fraction).
  - Better defined than the 0% radius, but depends on the filter/bandpass
- Uniform disk diameter
  - Fit of a uniform disk to the true intensity profile, e.g. the uniform disk that has the same integral flux as the true intensity profile.
  - Depends on filter/wavelength
  - Can be corrected to a limb-darkened/Rosseland radius using model atmospheres

Radius definitions

- Rosseland radius
  - Where the Rosseland-mean optical depth is 2/3 (or unity)
  - Not directly measurable, depends on model structure
  - Take the fitted 0% intensity radius and correct it by the factor between the (arbitrary) outermost model layer where the intensity is set to 0 and the layer where the Rosseland-mean optical depth equals 2/3 (or unity).
  - Most meaningful definition, corresponding to the definition of the effective temperature
  - Contaminated by extended molecular layers

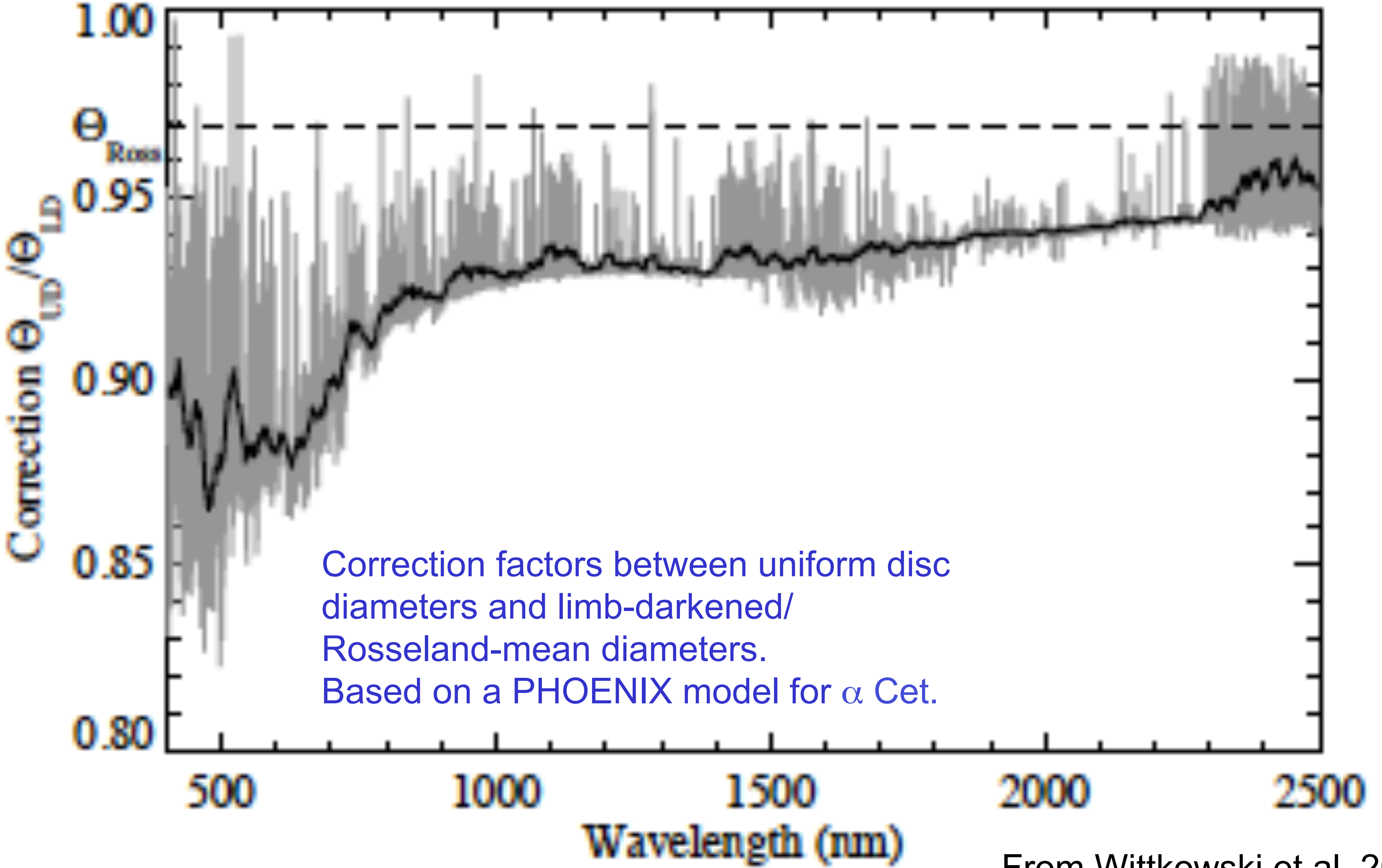

Correction factors between uniform disc diameters and limb-darkened/ Rosseland-mean diameters.
Based on a PHOENIX model for α Cet.

From Wittkowski et al. 2006

Methods probe the limb-darkening effect

- 2nd lobe visibility observations

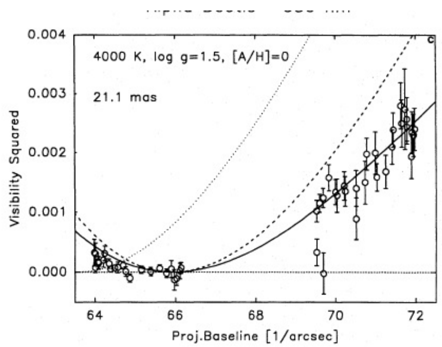

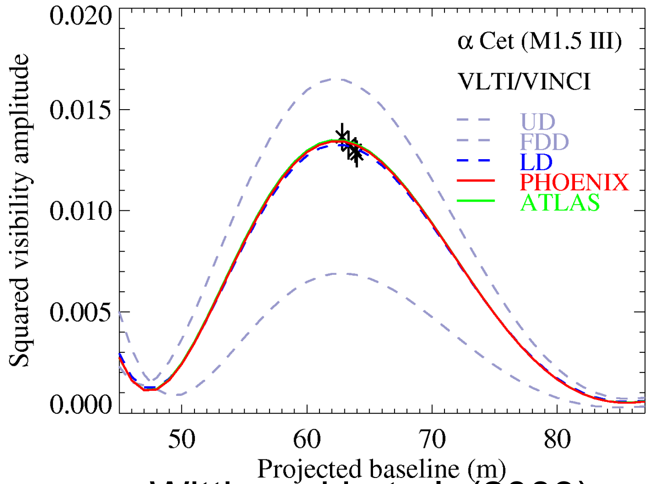

Wittkowski et al. (2003)

- UD diameter variation with wavelength

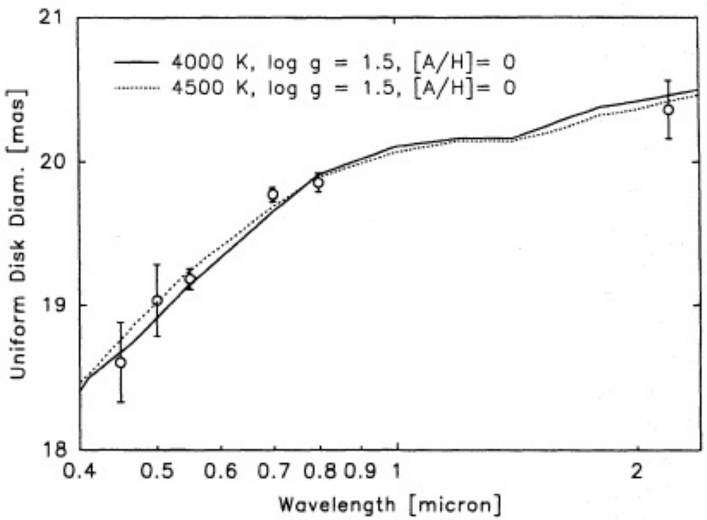

Quirrenbach et al. (1996)

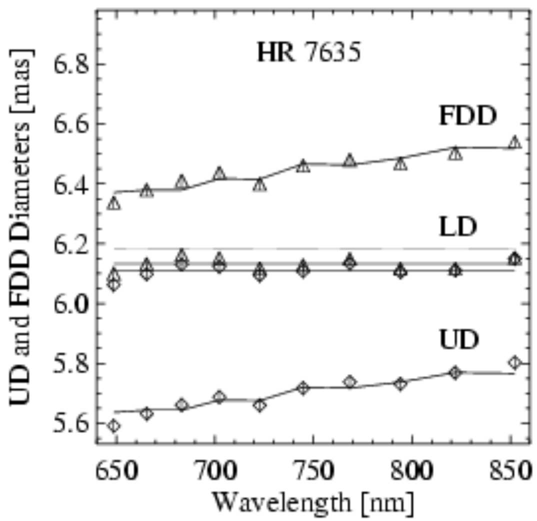

Wittkowski et al. (2001)

The limb-darkening effect for 3D model atmospheres

- Hotter, rising granules have a warmer temperature structure than cooler, descending dark lanes.
- The mean 3-D temperature structure differs from a1-D model and can be detected interferometrically via limb darkening (detected e.g. for Procyon by Aufdenberg et al. (2005).
- Asymmetric intensity profiles can in principle be interferometrically detected as well via the closure phases.

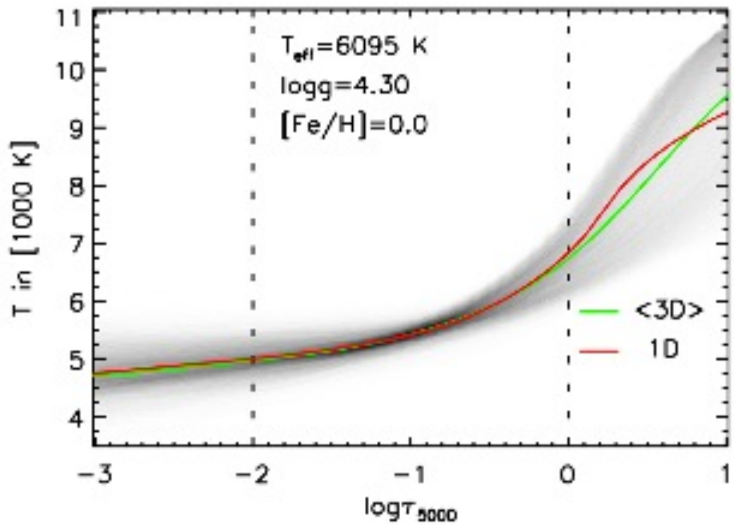

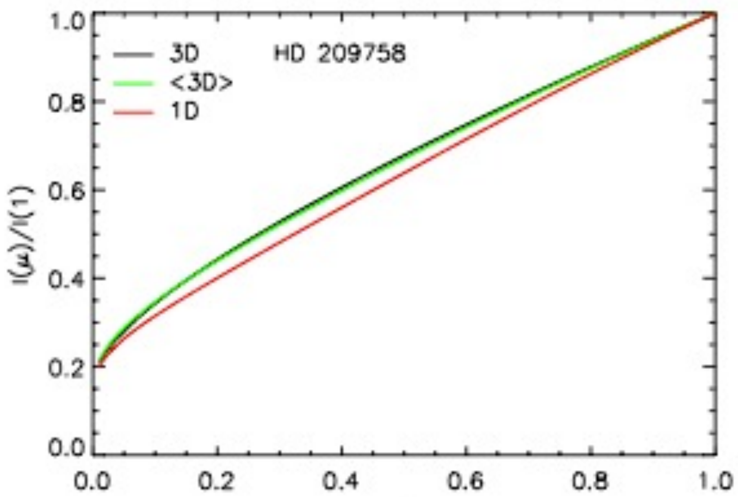

From Hayek et al. (2012)

Example 1: Interferometric (and spectroscopic) observations compared to PHOENIX model atmospheres

Menkar (alf Ceti): Observations

- *K*-band observations obtained with VLTI/VINCI in the first and second lobe of the visibility function (Oct-Dec 2003).
- UVES observations with dichroic settings 346+580 nm and 437+860 nm with spectral resolutions of 80000 and 110000.
- Bolometric flux from integrating spectro-photometry from the literature. Assumed E(B-V)=0.015.

  f_{Bol}=(1.03 +/- 0.07) 10^{-12} W/cm^2

Menkar (alf Ceti): Models

- PHOENIX code, version 13 (Hauschildt & Baron)
- Solar metallicity
- Micro-turbulence: 2 km/sec
- Tabulated flux from 300 nm to 1050 nm in steps of 0.001 nm
- Tabulated intensity profiles at 64 viewing angles from 1.8 to 2.5 μm in steps of 0.5 μm
- Corrected for air refraction index, Earth's motion and rotation, and radial velocity of Menkar. Broadened with v sini = 3 km/sec (mean for M0 giants).

Menkar (alf Ceti):
Comparison to spectro-photometry

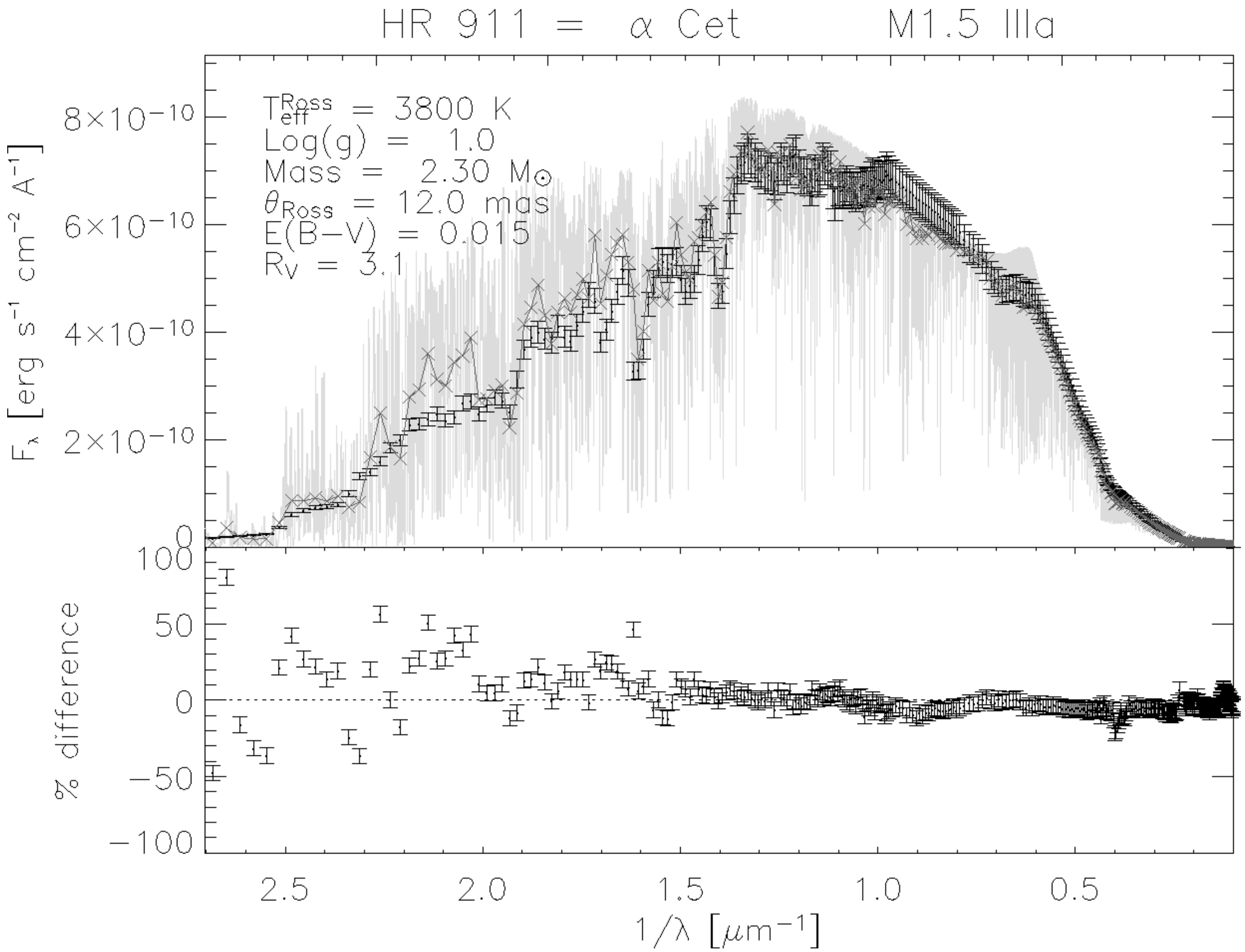

Menkar (alf Ceti): Comparison to interferometry

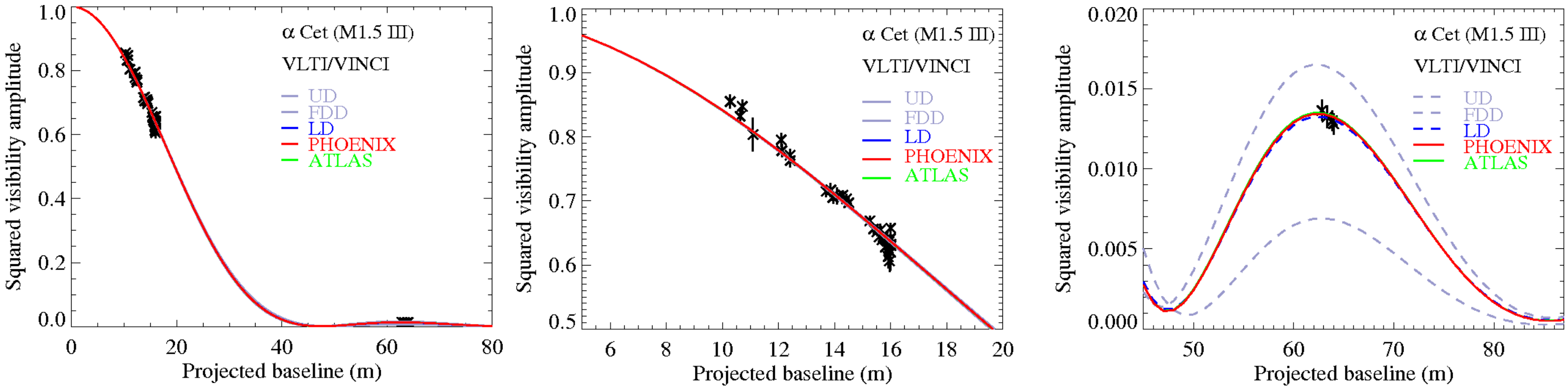

- Best-fitting 0% intensity diameters for a grid of PHOENIX models (outermost model layer)
- Rosseland diameters (where τ_{Ross}=1) computed from LD diameters based on the model

- Θ_{Ross} = 12.20 mas +/- 0.04 mas, virtually independent of the model of the grid
- T_{eff} = 3795 +/- 70 K with f_{bol}
- R_{Ross} = 89 +/- 5 R_{sun} with the Hipparcos parallax

- L=1460 +/- 300 L_{sun} from f_{bol} and π
- M=2.3 +/- 0.2 $M_{sun,}$ log g = 0.9 +/- 0.1 with evolutionary tracks

Menkar (alf Ceti): Comparison to UVES spectra

- TiO bandheads: 5598, 7054, 7088, 7126 A
- Atomic lines: Fe I (3683, 5447, 6945), Ca I (4227), Ti I (5966, 9675)
- Cross-correlation to obtain wavelengths shifts for each bandpass separately (bandpass ± 2 A)
- Continuum adjustment: two bandpasses blueward and redward of the bandpass (width 4 A, shift +6 A and -6 A)
- Comparison of χ^2 and equivalent width between observed and synthetic spectrum
- T_{eff} ~ 3820 ± 50 K, consistent with interferometry, log g not well constrained

Menkar (alf Ceti): Comparison to UVES spectra

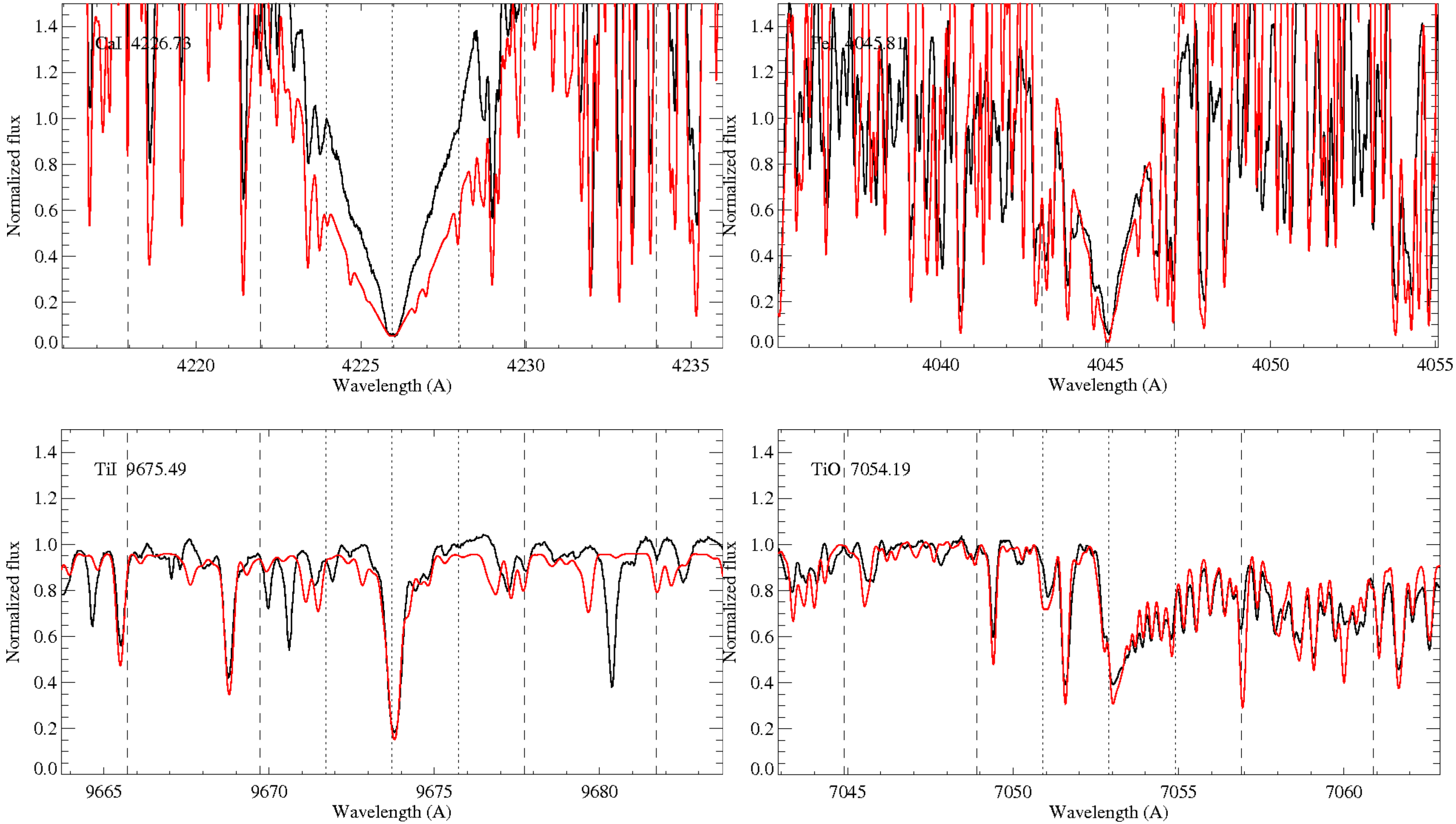

VLTI/VINCI observation of the M4 giant Ψ Phe

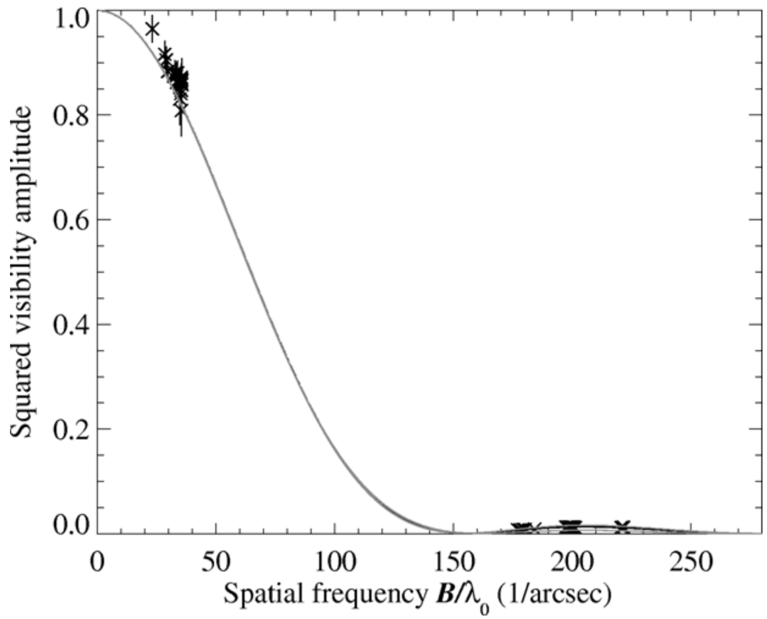

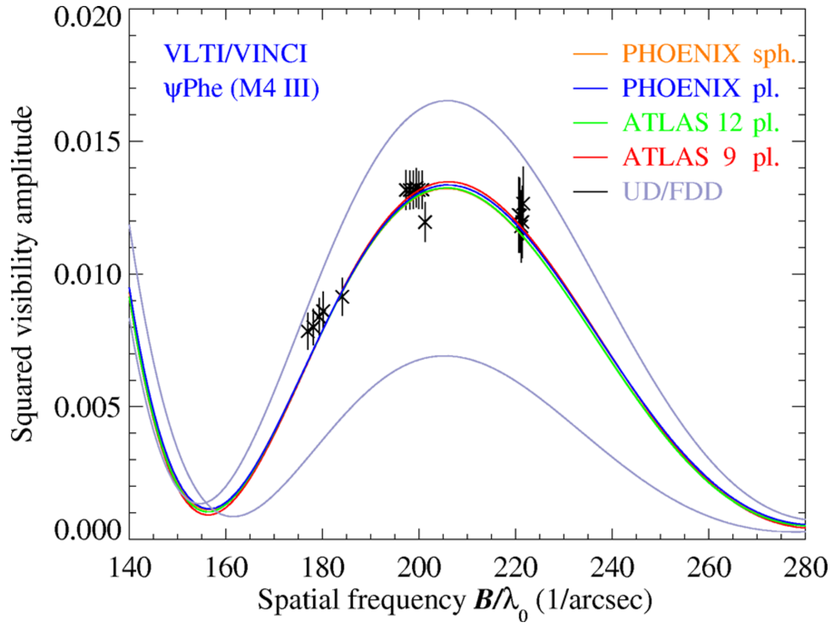

Stellar parameters:

θ_{Ross} = 8.13 +/- 0.20 mas

R_{Ross} = 86 +/- 3 R_{sun} (with parallax)

T_{eff} = 3550 +/- 50 K (with f_{bol})

M = 1.3 +/- 0.2 M_{sun}; log g = 0.68 +/- 0.11

Wittkowski, Aufdenberg & Kervella 2004

VLTI/AMBER observations of red supergiants

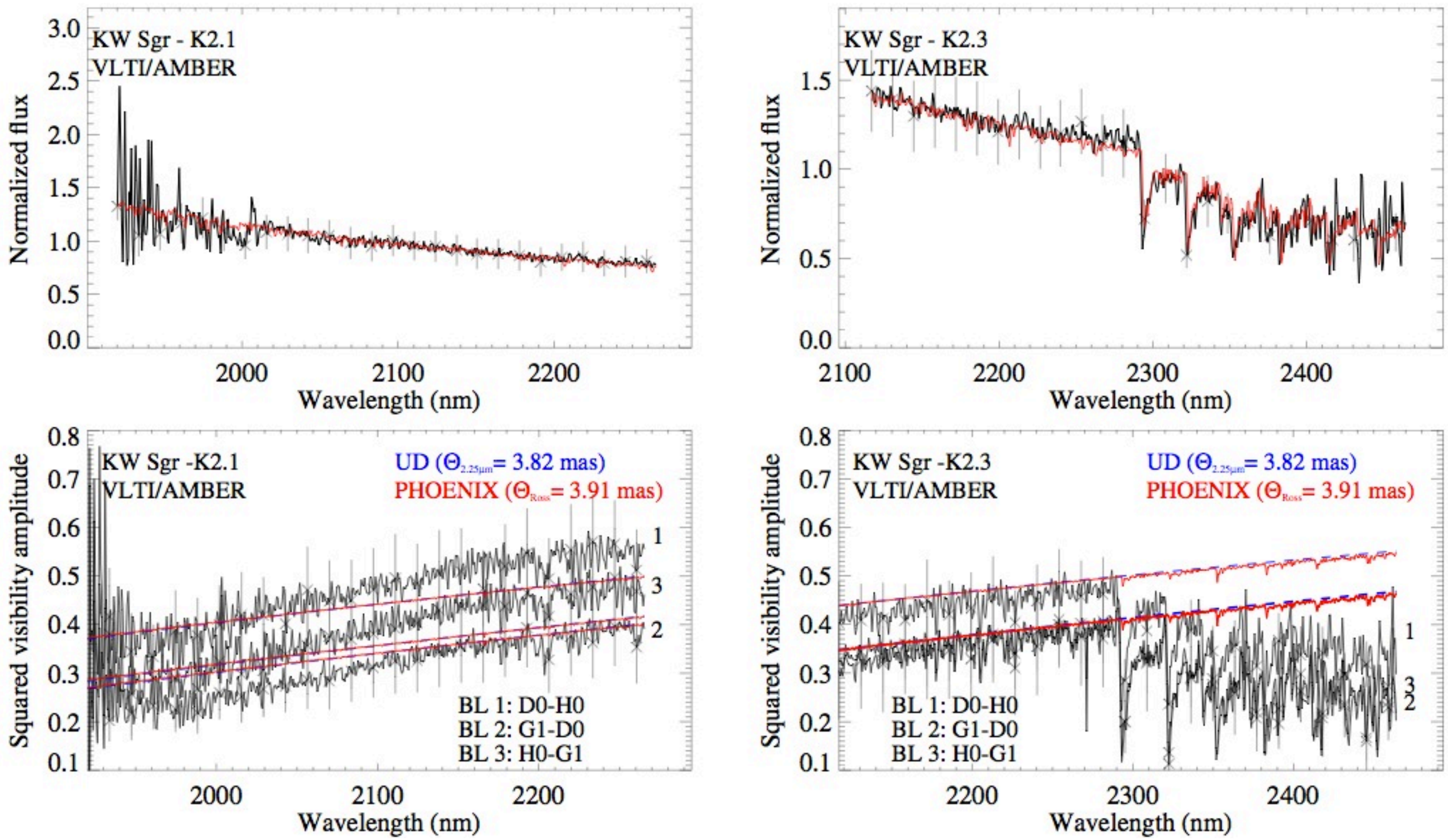

PHOENIX atmosphere models fit well the spectra, but do not predict the observed extensions of the atmosphere in the H2O and CO bands.
From Arroyo-Torres et al. (2013).

Extended atmospheres and molecular layers of AGB stars

CODEX model atmospheres

Evolutionary stage of AGB stars

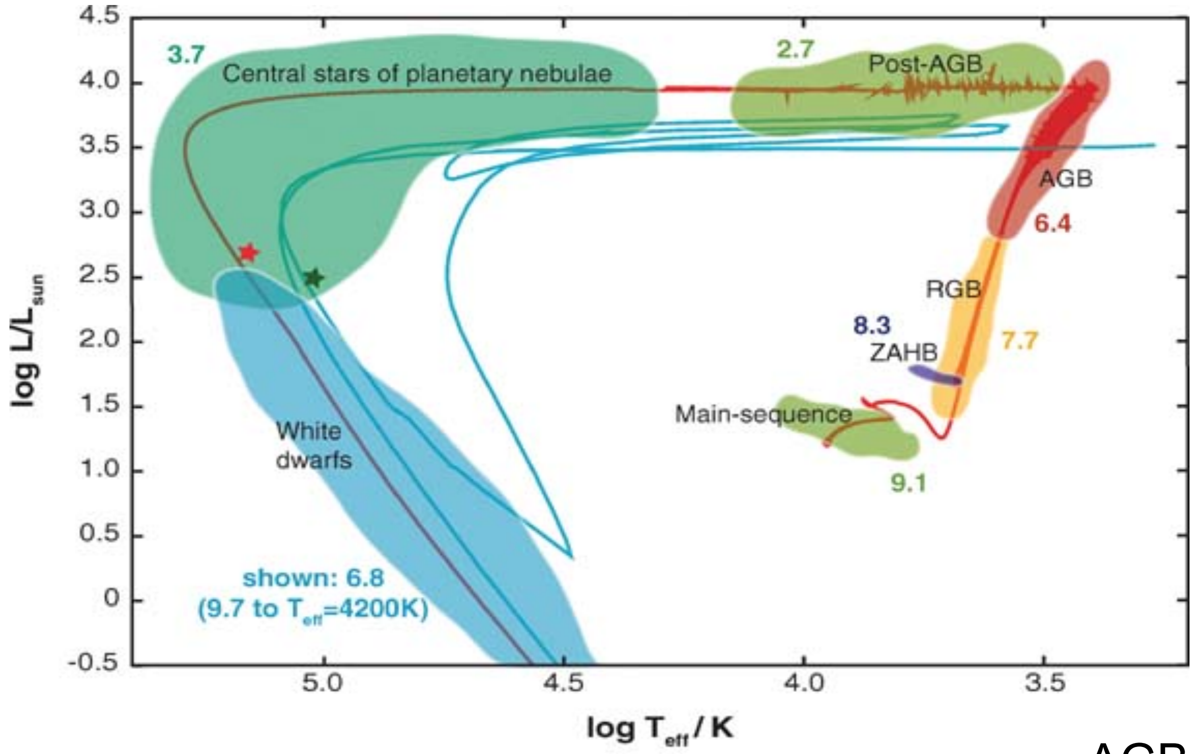

Two solar mass evolution track (Herwig 2005):

AGB stars represent the last stage of the evolution of low- to imtermediate mass stars that is driven by nuclear fusion. The most important driver for the further evolution is the mass-loss.

Stellar pulsation

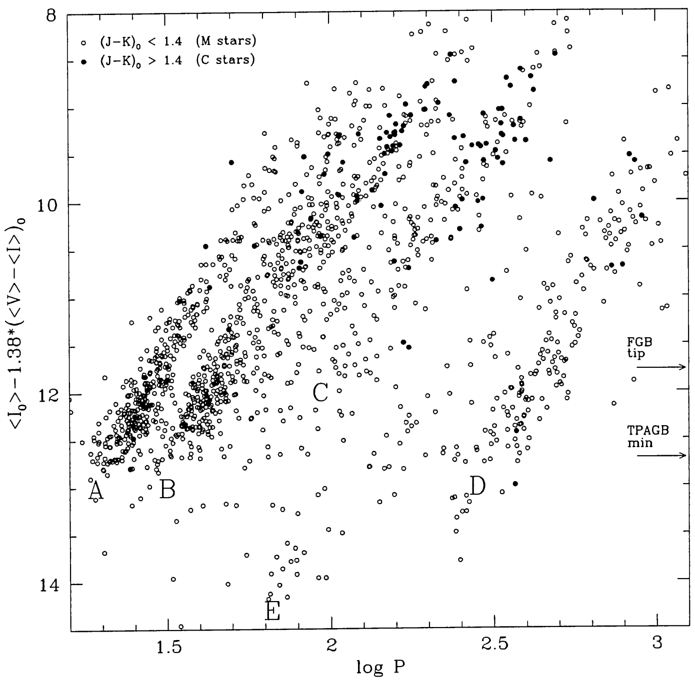

Figure 1. The period-luminosity relation for red variables. $<I>$ and $<V>$ are mean magnitudes, and P is in days. See text for details.

AGB stars are affected by stellar pulsations, starting with irregular pulsation in fundamental and mostly overtone modes on the low-luminosity AGB to regular pulsation in fundamental mode of Mira variables.

MACHO observations of LMC red giants (Wood et al. 1999):

Structure of an AGB star

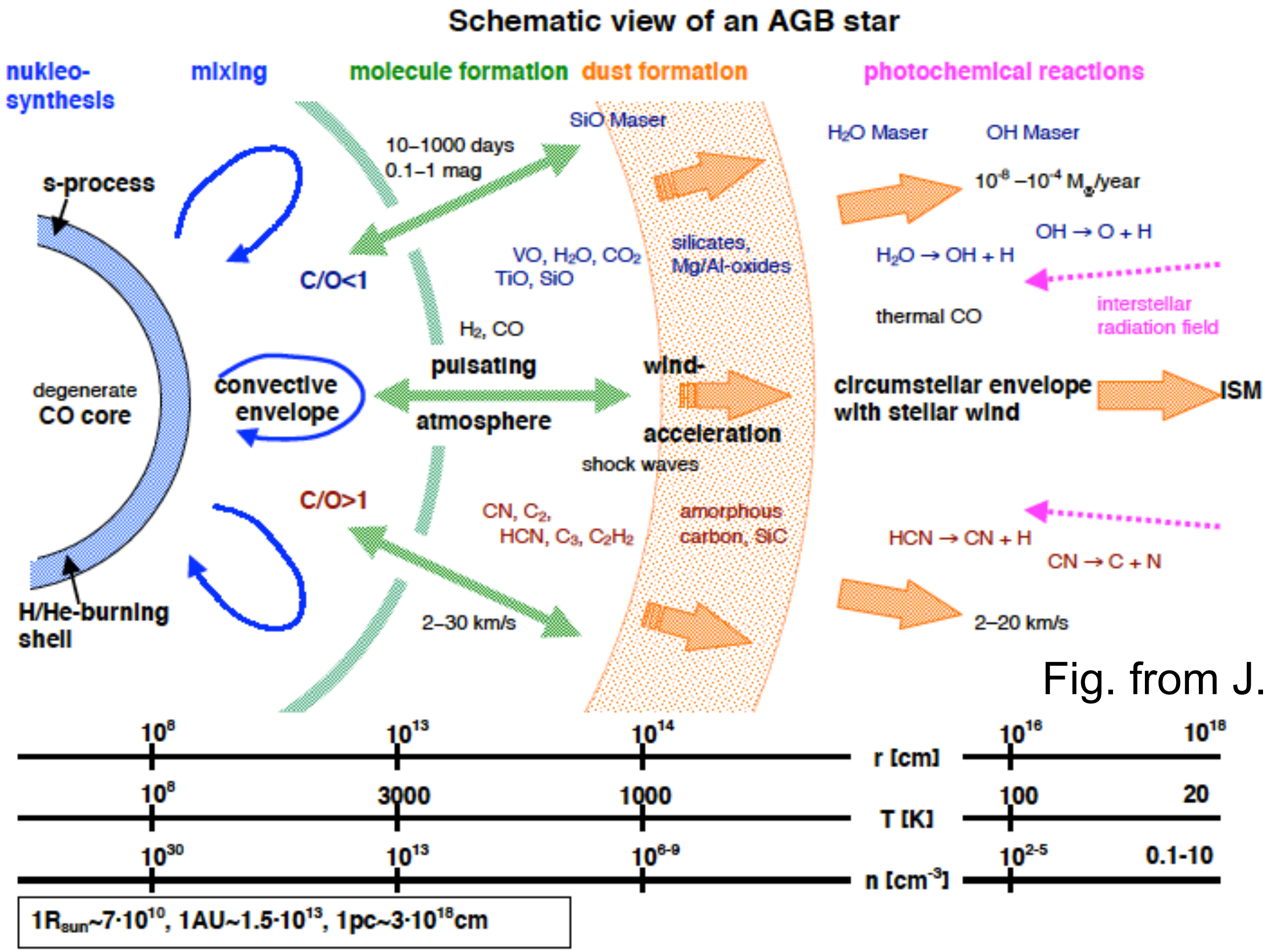

Fig. from J. Hron (after Le Bertre)

The mass-loss process is currently not understood for oxygen-rich stars.

Atmospheric structure of pulsating AGB stars

CODEX dynamic atmosphere models of Mira variables (Ireland et al. 2008, 2011):

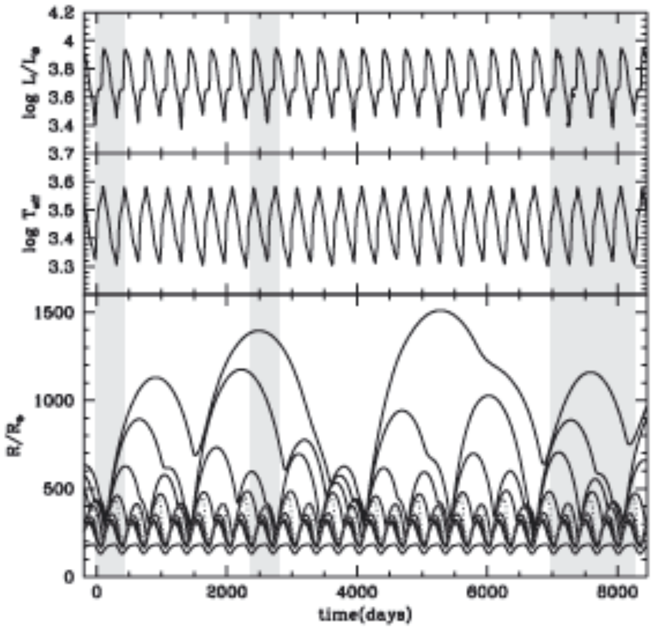

Figure 1. The luminosity (top panel), effective temperature (central panel) and radius of selected mass zones (lower panel) as a function of time for the *o54* pulsation model. The red dashed line in the bottom panel corresponds to the radius at Rosseland mean optical depth 2/3, and the effective temperature [$\propto (L/R^2)^{0.25}$] refers to this radius.

The pulsation in the stellar interior leads to atmospheric motion, which is regular near the Rosseland radius, but chaotic at mass zones further out (starting from 1.5-2 Rosseland radii).

Atmospheric structure of AGB stars

Pulsations and shock fronts lead to very complex and extended atmospheric intensity profiles with for example step-like shapes, and conditions favorable for the formation of molecules (for oxygen-rich stars most importantly H_2O and CO). Wavelength-dependent deviations from a uniform disk profile are predicted already in the first lobe of the visibility function.

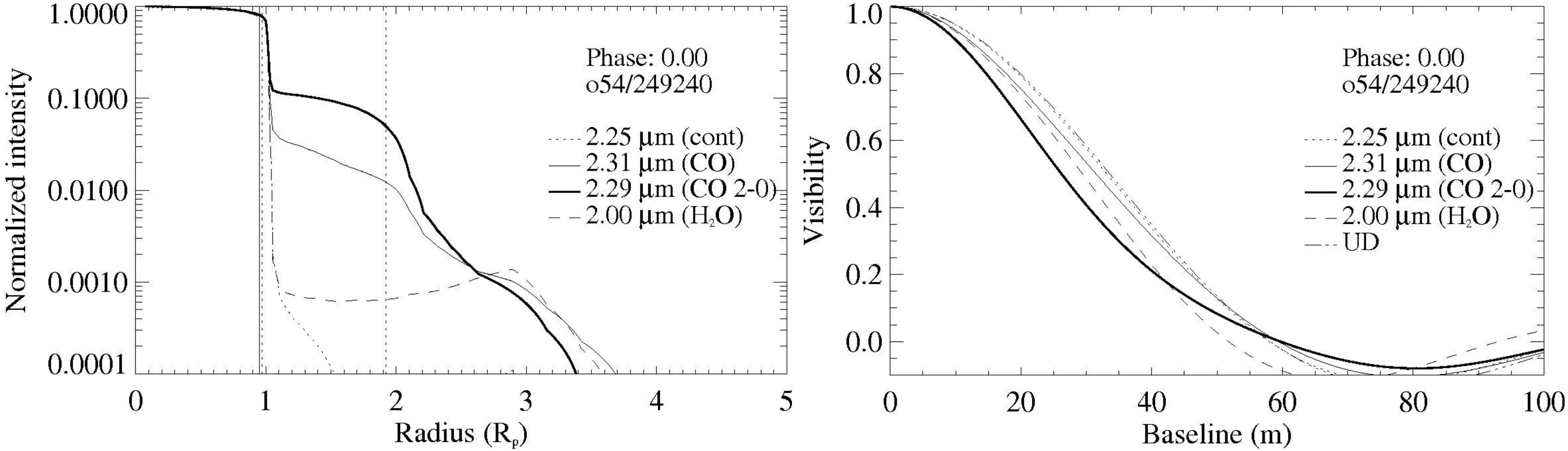

Dynamic CODEX models
(Ireland et al. 2008, 2011)

LR AMBER observation of the Mira variable S Ori

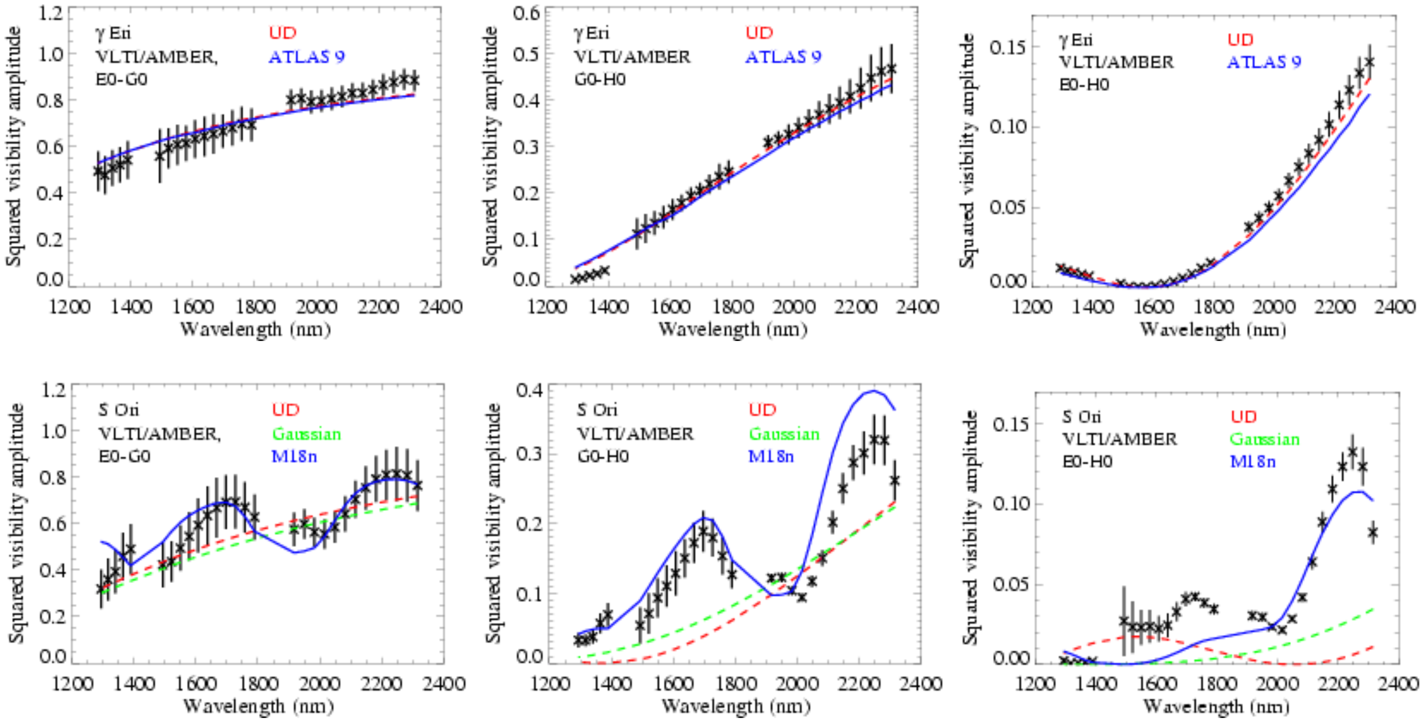

M giant

Mira

The bumpy visibility curve is a signature of molecular layers lying above the photosphere.

At some wavelengths, the molecular opacity is low, we see the photosphere, the target appears smaller.

At other wavelengths, the molecular opacity is larger, we see the water shell, the target appears larger.

AMBER allows us to probe different layers of the extended atmosphere.

Visibility and UD diameter variations with wavelength resemble reasonably well the predictions by dynamic model atmospheres including molecular layers, in particular water vapor and CO.

Wittkowski, et al. 2008

Comparison of MR AMBER observations of Mira variables to new dynamic model atmospheres (CODEX models by Ireland, Scholz, & Wood 2008 and 2011

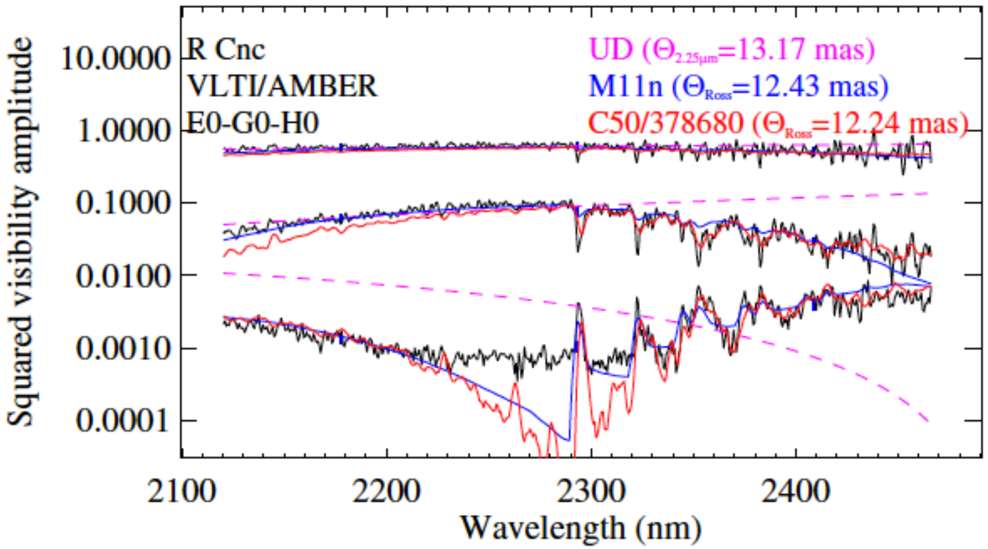

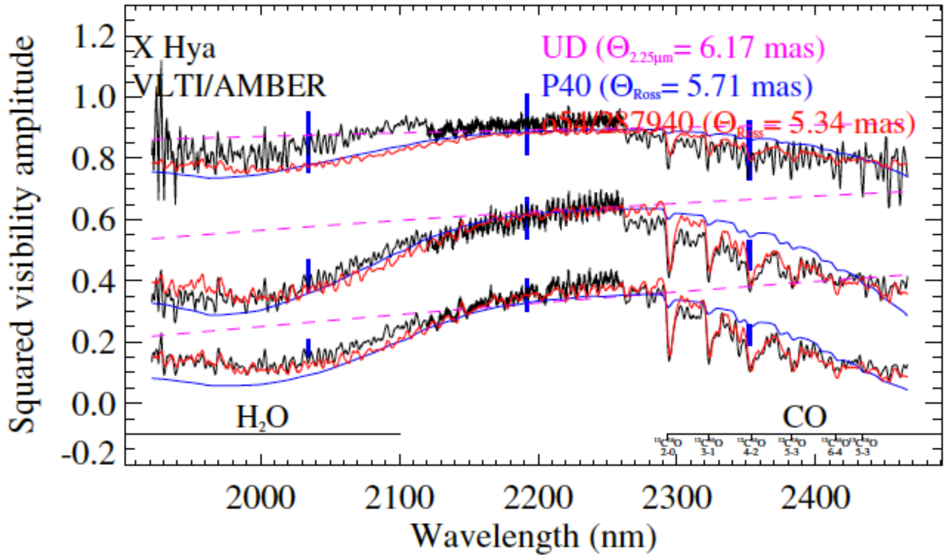

Visibilities are well consistent with predictions by the latest dynamic model atmosphere series based on self-excited pulsation models and including atmospheric molecular layers. Best-fit parameters (phase, T_{eff}, distances) consistent with independent estimates. Teff also determined from best-fit angular diameter and simultaneous SAAO photometry.

Wittkowski et al. 2011

Uniform disk diameter and intensity profiles

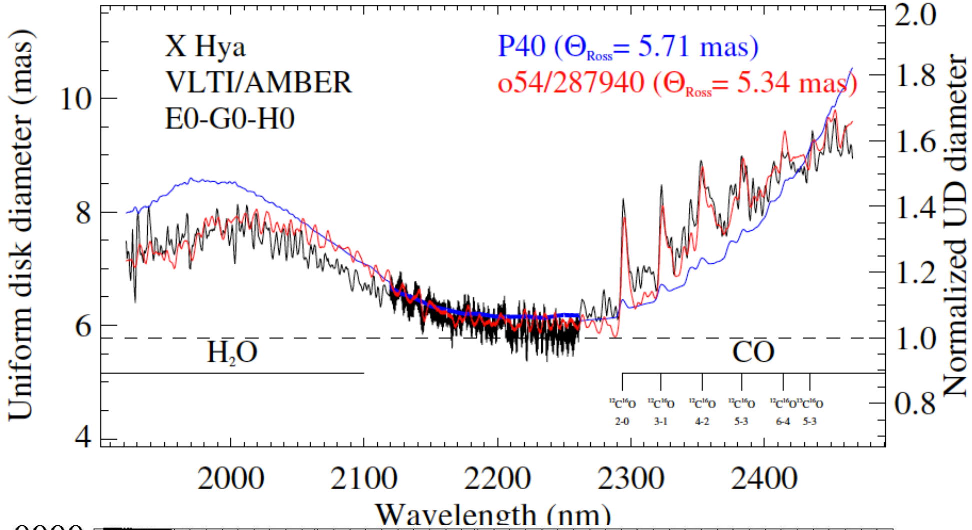

What does this mean ?

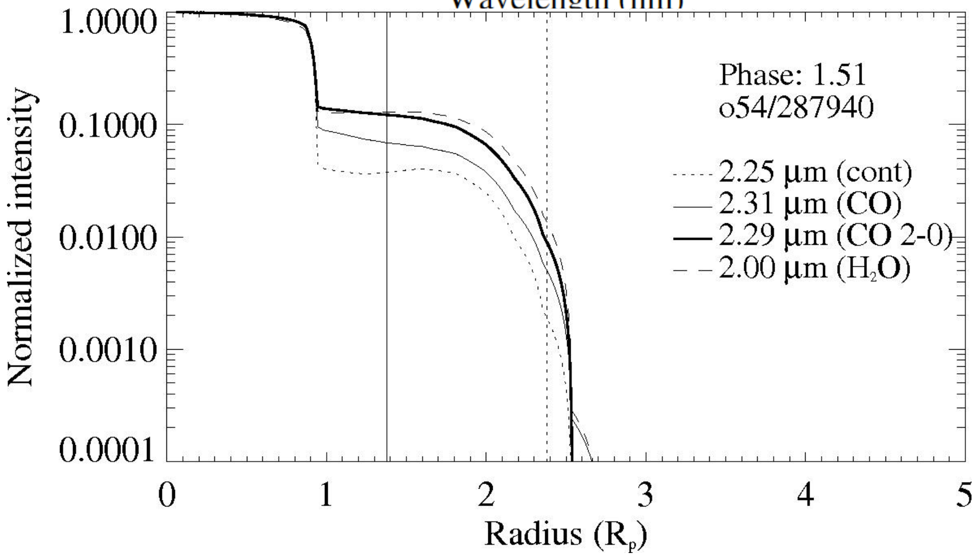

Not much ?

Some qualitative indication
of more intensity in outer layers ?

We are far beyond measuring "uniform disk" "radii" of stars.

Wavelength-dependent closure phases

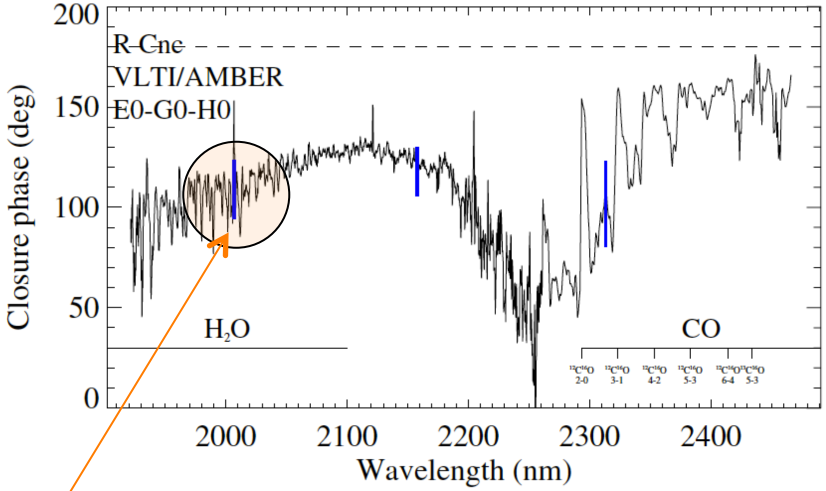

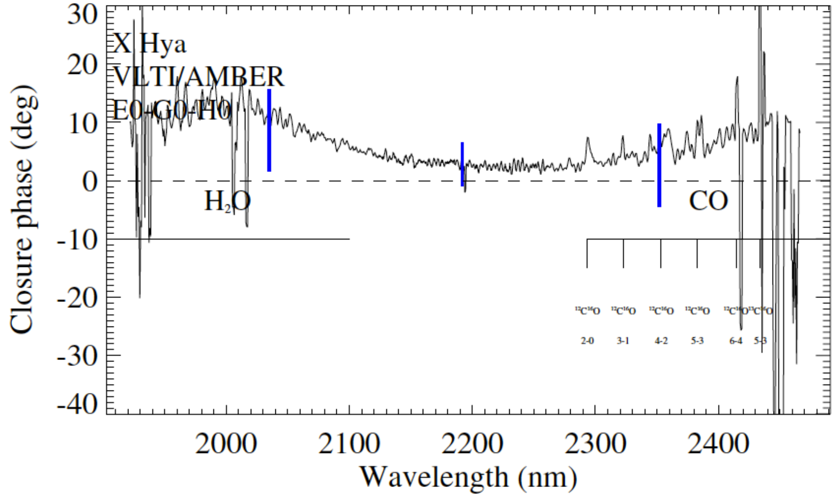

For example, one unresolved spot at separation 4 mas contributing 3% of the total flux

Wavelength-dependent closure phases indicate deviations from point symmetry at all wavelengths and thus a complex non-spherical stratification of the atmosphere. In particular, the strong closure phase signal in the water vapor and CO bandpasses is interpreted as a signature of large-scale inhomogeneities/clumps of molecular layers.

These might be caused by pulsation- and shock-induced chaotic motion in the extended atmosphere as theoretically predicted by Icke et al. (1992) and Ireland et al. (2008, 2011).

May be important for non-LTE chemistry and the origin of asymmetric CSE shapes.

Wittkowski et al. 2011